Journal of Applied Physics ARTICLE pubs.aip.org/aip/jap

High-temperature annealing induced electrical compensation in UID and Sn doped β-Ga_2O_3 bulk samples: The role of V_{Ga}–Sn complexes

Cite as: J. Appl. Phys. **137**, 055703 (2025); doi: 10.1063/5.0249111
Submitted: 15 November 2024 · Accepted: 14 January 2025 ·
Published Online: 5 February 2025 · Publisher error corrected: 10 February 2025

H. J. von Bardeleben,[1,a] Xuanze Zhou,[2,a] Jingbo Zhou,[2] Guangwei Xu,[2] Shibing Long,[2] and U. Gerstmann[3,4]

AFFILIATIONS

[1]Institut des NanoSciences de Paris (INSP), Sorbonne Université, 4 place Jussieu, Paris 75005, France
[2]School of Microelectronics, University of Science and Technology of China (USTC), Hefei 230026, China
[3]Theoretical Materials Physics, University of Paderborn, Pohlweg 55, Paderborn 33098, Germany
[4]Quantum Materials Modelling, Department of Physics, University of Paderborn, Paderborn 33098, Germany

[a]**Authors to whom correspondence should be addressed:** vonbarde@insp.jussieu.fr and zhouxz@ustc.edu.cn

ABSTRACT

By electron paramagnetic resonance (EPR) and photoluminescence spectroscopy, we have investigated the effect of high-temperature annealing under oxygen atmosphere on the electrical and defect properties of unintentionally doped (UID) and highly doped (Sn) n-type bulk samples of β-Ga_2O_3. The EPR analysis of the shallow donor concentration shows efficient electrical compensation in the Sn doped β-Ga_2O_3 samples but only marginal changes for the UID samples. In the Sn doped samples, we observe the formation of a Ga vacancy related acceptor defect responsible for the compensation. Its spin Hamiltonian parameters are electron spin $S = 1/2$, g-tensor $g_{11} = 2.0423$, $g_{22} = 2.0160$, $g_{33} = 2.0024$, and hyperfine interaction (hf) with two equivalent Ga atoms with $A(^{69}Ga) = 28$ G. To identify its microscopic structure, we have performed *first-principles* calculations of the EPR parameters and the associated photoluminescence spectra of different Ga vacancy–Sn donor complexes, including a simple nearest neighbor pair V_{Ga}–Sn_{Ga}. From these calculations, we attribute this V_{Ga} defect to a negatively charged split vacancy complex V_{Ga1}–Sn_{ib}–V_{Ga1}. This V_{Ga} defect is different from the irradiation induced V_{Ga} center.

INTRODUCTION

The modification of the structural, optical, and electrical properties of n-type conducting β-Ga_2O_3 by high-temperature annealing has been reported in various studies.[1–7] High-temperature annealing is a standard approach in semiconductor technology. High-temperature annealing has been applied for two *a priori* contradictory purposes: (i) the transformation of n-type conductive layers in high resistive ones or (ii) on the contrary to increase the carrier concentration in n-type doped samples. It is equally applied after ion implantation for dopant activation and annealing of structural damage.[8–10] It has recently been applied for the optimization of enhancement mode β-Ga_2O_3U-shaped trench vertical MOSFETS[5] to obtain high resistive layers. These annealing were performed in the temperature range of 900–1200 °C under either O_2 or N_2 atmospheres and have been applied to thin films and also to bulk samples. The importance of the nature of the shallow donor (SD), Si or Sn, has not been investigated; both give rise to shallow effective mass donors but occupy different lattice sites. Si is a shallow donor when substituting on a fourfold coordinated Ga1 site, whereas Sn is a shallow donor on a sixfold coordinated Ga_2 lattice site. It may seem surprising that high-temperature annealing in the same temperature range can be used to reduce and increase the carrier concentration. For example, Tadjer *et al.*[1] reported the effect of 3 h annealing of Si and Sn doped EFG bulk samples in either N_2 or O_2 atmospheres, which showed an increase in the carrier concentration for annealing at 1000 °C under N_2, whereas a strong reduction was observed for annealing under O_2 at 1150 °C. The formation of intrinsic acceptors is generally evoked to explain the compensation, and we have shown

recently that indeed Ga vacancy defects are responsible for the electrical compensation.[2]

The standard techniques in electrical measurements, Hall effect, and deep level transient spectroscopy (DLTS) cannot identify the microscopic structure of the annealing induced defects. For example, a number of electron traps at E_C—0.62 eV, E_C—0.82 eV, E_C—1.00 eV, E_C—2.16 eV, E_C—4.40 eV have been evidenced in EFG grown bulk samples, but without clear identification.[11] We have shown recently[2] by EPR spectroscopy that a V_{Ga} related defect is responsible for the electrical compensation by high-temperature annealing. EPR spectroscopy is a useful complementary approach for such studies,[12–20] as it identifies equally the chemical nature of the defects and allows a quantitative analysis by spin counting. EPR spectroscopy, which can be applied to thin films as well as bulk samples, is a volume sensitive technique and analyzes the total volume of bulk and thin film samples. Various extrinsic defects such as Ir, Mg, Zn, Fe, Cu, Ni as well different V_{Ga} related centers have been investigated in β-Ga_2O_3 by EPR. Some of them (Fe, Cr, Cu) are present as native defects in the EFG grown bulk materials and lead to partial compensation. In specific charge states (Fe^{3+}, Cr^{3+}, Cu^{2+}), they are paramagnetic and can be analyzed by EPR. The main parameters determined in EPR experiments are the electron spin S, Landé g-tensor, the central and distant hyperfine interaction and the point symmetry; these parameters can be compared to *first-principles* calculations and allow to build a microscopic model. In the wide-bandgap semiconductor Ga_2O_3, these defects have more than one charge transition level and their charge states can be used to monitor the Fermi-level position.

Our previous results[2] have already shown that the effects of the annealing are not limited to a micron-thick surface layer but modify the properties in the entire volume of typically 600 μm thick bulk samples. In this work, we have investigated the effect of high-temperature annealing of 650 μm thick substrates for two different series of samples: UID doped (−201) and Sn doped (001) oriented bulk samples with carrier concentrations of 2×10^{17} and 5×10^{18} cm^{-3}, respectively.

EXPERIMENTAL DETAILS

UID doped (−201) and Sn doped (001) oriented 650 μm thick bulk samples have been purchased from Novel Crystal Technology. The carrier concentrations were, respectively, $(N_D - N_A) = 2 \times 10^{17}$ cm^{-3} and $(N_D - N_A) = 5 \times 10^{18}$ cm^{-3}. The samples were cut in 5×6 mm^2 pieces and were furnace annealed under O_2 atmosphere at T = 900 °C, T = 1000 °C, T = 1100 °C, 1200 °C for 6 h. The samples were heated to the annealing temperatures at a rate of 5 °C/min and cooled under the same conditions.

The EPR measurements were performed with a Bruker X-band spectrometer in the temperature range of T = 4 K and T = 300 K. We applied standard 100 kHz field modulation, which results in first-derivative Lorentzian or Gaussian EPR lineshapes. Spin concentrations were determined by double integration of the EPR spectrum and comparison with a spin standard sample (Cr: Al_2O_3) purchased from the National Bureau of Standards (NBS). The EPR spectra were taken under thermal equilibrium conditions and under low temperature *in situ* photoexcitation with a UV Hg light source. The EPR spectra are simulated with the EasySpin program using Gaussian lineshapes. The photoluminescence spectra were taken at T = 4 K with a UV excitation (266 nm).

COMPUTATIONAL METHOD

The EPR parameters of different V_{Ga}–Sn complexes were calculated by density functional theory (DFT) calculations using the Quantum ESPRESSO package[21,22] in their EPR active ($S = 1/2$) singly negative charge state. In particular, we calculated the g tensor and the hyperfine (hf) interactions with the neighboring Ga nuclei. The defect structures (ground states, excited states as well as Slater–Janak transition states) are modeled within periodic boundary conditions using 160 atom containing supercells, and a $2 \times 2 \times 2$ Monkhorst–Pack k-point sampling, norm-conserving pseudopotentials and a plane-wave basis set with a 950 eV energy cutoff. All defect structures are fully relaxed (forces below 10^{-4} Ry/Bohr) using the standard HSE hybrid functional[23] to describe the exchange-correlation interaction of the many-particle system. For the HSE-relaxed structures, the EPR parameters are calculated within linear magnetic response using the gauge-including projector-augmented wave (GIPAW) method[24,25] and using the semi-local PBE functional.[26] This combined HSE-PBE approach yields highly accurate hf splittings but tends to underestimate the deviation of the elements of the electronic g tensor.

EXPERIMENTAL RESULTS AND DISCUSSION

Shallow donor properties

EPR spectroscopy can be applied to the study of conduction electrons (CEs), the so-called conduction electron spin resonance (CESR), shallow donors and to paramagnetic centers such as intrinsic point defects. The distinction between CESR and SD EPR spectroscopy has to be taken into account for the determination of defect concentrations as CE follow a Pauli-like magnetism whereas paramagnetic defects have a Curie-like magnetism. For n-type conducting samples doped with Si or Sn shallow donors with respective ionization energy of $E_D = 36$ meV or 56 meV, the donors will be ionized at T = 300 K and magnetic resonance will measure the CESR. At temperatures below T < 60 K, the carriers will freeze out and the paramagnetic, neutral shallow donors can be quantitatively analyzed.

The neutral shallow donors and conduction electrons in β-Ga_2O_3 have been studied previously by different authors.[27–32] Their spin Hamiltonian parameters have been determined as electron spin $S = 1/2$, g-tensor with principal values of $g_{11} = 1.9572$, $g_{22} = 1.9602$, and $g_{33} = 1.9622$ with the g_{22} aligned with the crystal b axis. Contrary to the case of transition metal impurities, the EPR linewidth of SD is extremely temperature dependent due to motional narrowing. This occurs when the donor electrons are delocalized in an impurity band or are thermally emitted in in the conduction band. We have shown previously that the EPR donor linewidth can be used for the analysis of the electrical transport properties and gives insight the variable range hopping conduction observed in n-type Ga_2O_3.[27,28] Typical experimental EPR linewidth are $\Delta B < 1$ G at T = 300 K and $\Delta B = 60$ G at T = 4 K, if the carriers are fully localized.[28] This unusual behavior has been analyzed in more detail in Ref. 28 and described to thermally activated delocalization of the donor electrons and variable range hopping transport at intermediate temperatures.

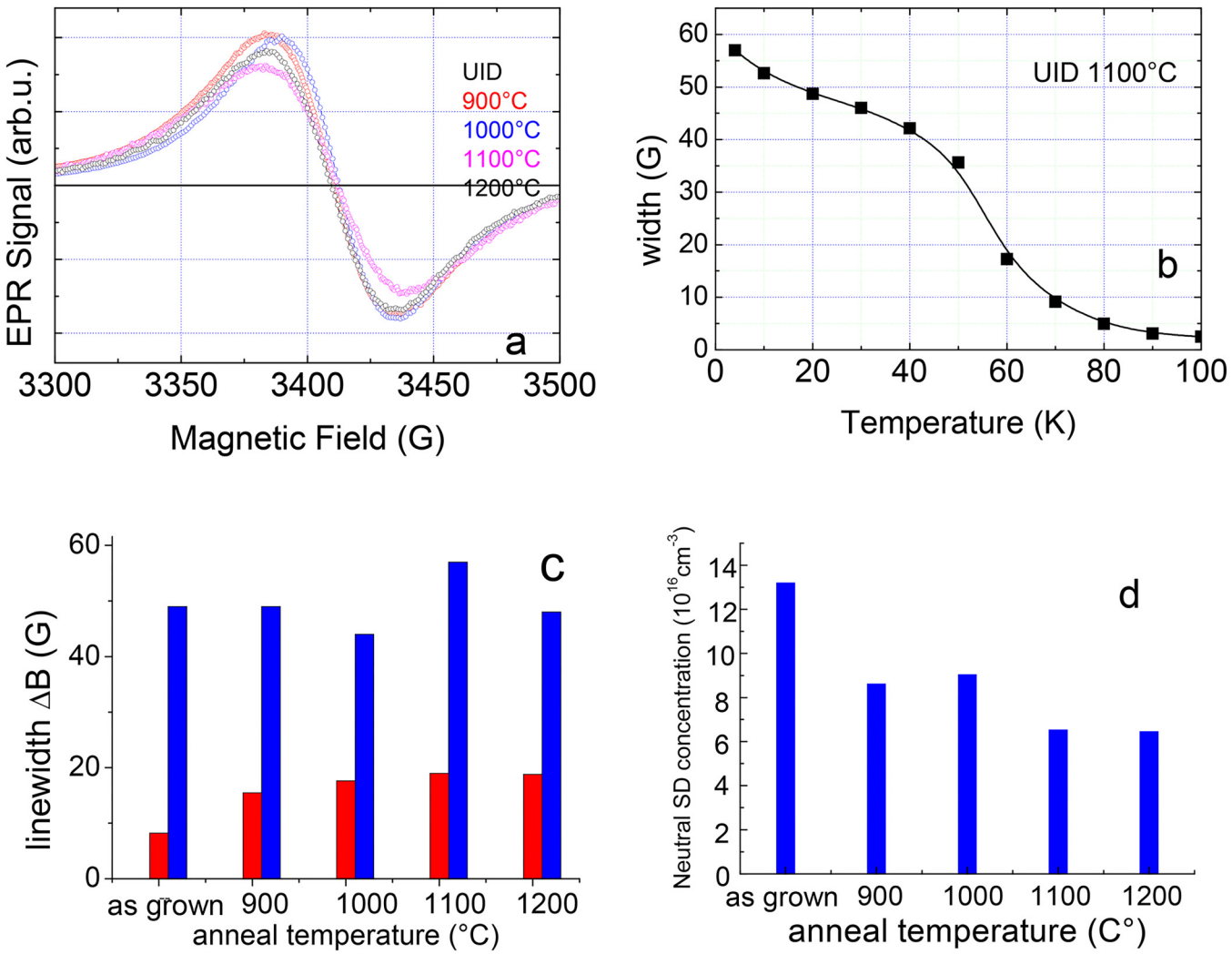

FIG. 1. EPR results of the SD for the UID samples annealed at 900, 1000, 1100, 1200 °C: (a) EPR spectra at T = 4 K showing a constant linewidth of ∼50 G irrespective of the annealing temperature, (b) linewidth ΔB as a function of temperature for the 1100 °C sample (c) linewidth at T = 60 K (red) and T = 4 K (blue) for the as grown and annealed samples, and (d) neutral SD concentrations at T = 4 K for the as grown and annealed samples.

UID samples

In Fig. 1(a), we show SD EPR spectra at T = 4 K for the UID samples annealed at 900, 1000, 1100, 1200 °C, respectively. The EPR spectra were taken under identical conditions and we observe comparable intensities and linewidth irrespective of the annealing temperature. At T = 60 K [Figs. 1(b) and 1(c)], the linewidths are in the range of 15–18 G, which demonstrates that the donor electrons are still mobile and not yet fully localized. At T < = 40 K, the linewidth increases further up to 60 G. At T = 4 K, the donor electrons are fully localized given the thermal ionization energy of the effective mass donor of $E = 36$ meV. By a double integration of the donor signals at T = 4 K, we obtain the spin concentration [Fig. 1(d)]. We observe within the error bars a decrease by 40% to 1.3×10^{17} cm^{-3} for the 900 and 1000 °C annealed samples and a further 20% decrease after the 1100 and 1200 °C annealing. Surprisingly, the annealing has only slightly reduced the neutral donor concentration from 1.7×10^{17} to 0.8×10^{17} cm^{-3} and the samples are still *n*-type conductive at T = 300 K.

Sn doped samples

In Fig. 2(a), we show the shallow donor EPR spectra at T = 4 K for the Sn doped Ga_2O_3 samples for the different annealing temperatures. The linewidth increases [Fig. 2(b)] with the annealing temperature, indicating increased electrical compensation. But only for the 1200 °C annealed sample has the linewidth increased to ΔB = 60 G, demonstrating that the carriers are fully localized. In Fig. 2(c), we show the variation of the EPR linewidth with

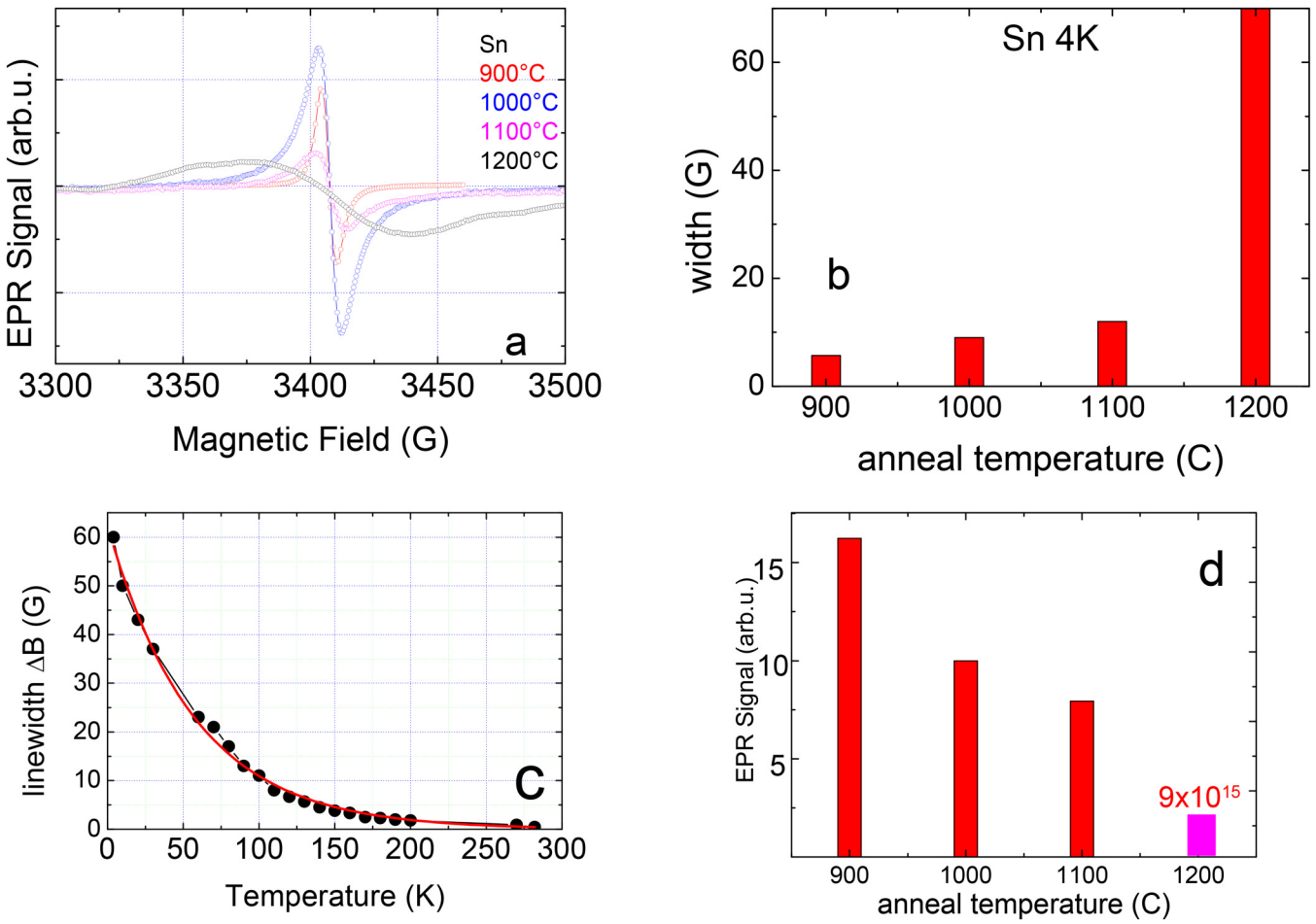

FIG. 2. EPR results of the SD for the Sn doped samples annealed at 900, 1000, 1100, 1200 °C. (a) comparison of the SD EPR spectra at T = 4 K as a function of annealing temperature; (b) SD linewidth at T = 4 K as a function of annealing temperature, (c) SD linewidth as a function of temperature for the 1200 °C annealed sample and fit with a single exponential; (d) (red) SD concentration at T = 4 K obtained by double integration of the EPR spectra; for the 900, 1000, 1100 °C annealed samples the concentration is given in in arbitrary units as the donor is not yet localized, (magenta) absolute spin concentration (spin/cm^3) for the 1200 °C annealed sample.

temperature for the 1200 °C annealed sample. Its variation is different from the case of the UID doped samples, which will be analyzed in more detail in another paper. In Fig. 2(d), we compare the SD concentrations measured at T = 4 K. We observe a monotonous decrease but as the donor electrons are still not localized only relative concentrations can be measured. In the 1200 °C annealed sample, the linewidth of 60 G shows complete localization and thus the spin concentration can be quantitatively determined by comparison with a spin standard sample. We obtain a value [Sn°] $=0.9 \times 10^{16}$ cm^{-3}. Thus, the neutral SD concentration has been reduced from initially 5×10^{18} cm^{-3} by two orders of magnitude.

Annealing induced defects: V_{Ga}

In the UID samples, no new paramagnetic defect is observed after the annealing. This is different from the Sn doped samples, in which a V_{Ga} related paramagnetic defect is generated by the annealing. The fingerprints of paramagnetic V_{Ga} centers are a spin S = 1/2, g-values $g > 2.00$, typical for oxygen hole centers, and strong hyperfine interaction with neighboring Ga atoms. Intrinsic V_{Ga} centers are triple acceptors and could thus efficiently compensate n-type samples. Their detection by EPR requires the (2−) charge state and thus particular Fermi-level positions. If the Fermi-level is pinned on the (3−/2−) level, this defect can be observed at thermal equilibrium by EPR in the paramagnetic 2− charge state with $S = 1/2$. Its observation after 1000 °C annealing indicates a shift of the Fermi-level to about E_C—2.0 eV.

In Fig. 3(a), we show for the 1000 °C annealed sample the experimental EPR spectrum of the V_{Ga} related defect and its simulation with the EasySpin program. We obtain the following spin Hamiltonian parameters: electron spin $S = 1/2$, principal values of the g-tensor: $g_{11} = 2.0423$, $g_{22} = 2.0160$, $g_{33} = 2.0024$ and a hyperfine

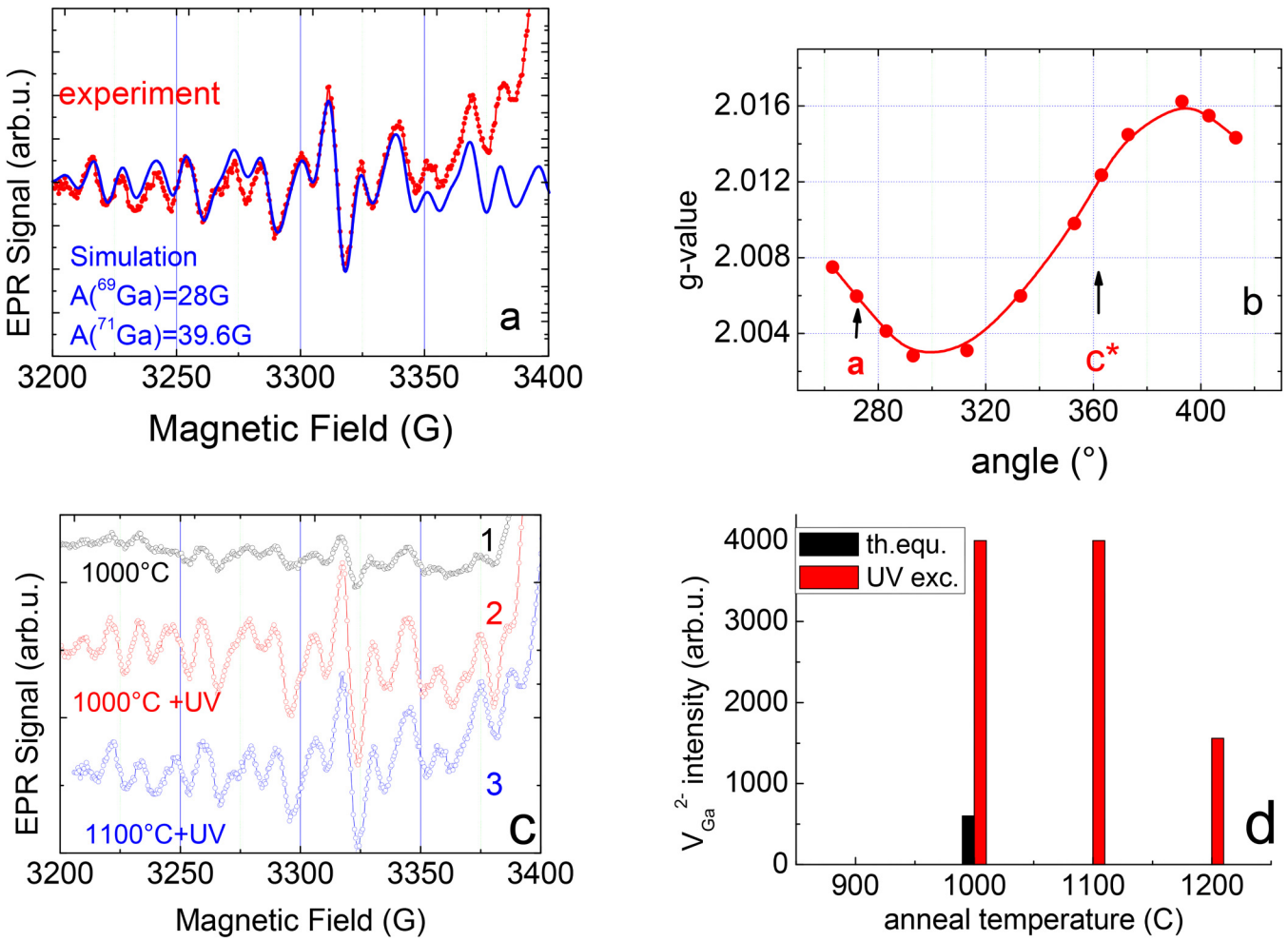

FIG. 3. (a) Sn1100 sample, EPR spectrum of the V_{Ga} center at T = 60 K, red points experiment, blue line simulation with parameters given in the text, the magnetic field is applied in-plane 40° from c* (b) angular variation of the resonance fields of the V_{Ga} spectrum in the (a)–(c) plane. (c) Sn1000 sample, V_{Ga} spectra at thermal equilibrium (1) and after photoexcitation (2) and V_{Ga} spectrum after photoexcitation for the Sn1100 sample (3), the magnetic field is applied in-plane 40° from c*; (d) V_{Ga} spin concentration in thermal equilibrium (black) and after UV photoexcitation (red).

interaction with two equivalent Ga atoms with A(^{69}Ga) = 29 G. As the Ga atoms have a nuclear spin $I = 3/2$ and two isotopes (^{69}Ga, ^{71}Ga) with different nuclear moments and isotopic abundances of 60% and 40%, respectively, the hf interaction with two Ga atoms gives rise to a characteristic multiplet structure. It should be stressed that the spin Hamiltonian parameters are different from the ones reported for the irradiation induced V_{Ga} centers.[33] In Fig. 3(b), we show the angular variation of the V_{Ga} center in the crystal **b** plane, from which the g-values g_{22} and g_{33} are obtained. The third value g_{11} is obtained from a measurement with the magnetic field aligned B//**b**. The Sn doped samples become increasingly compensated with the annealing temperature, which would *a priori* imply an increased V_{Ga} concentration. However, the EPR intensity of the (2−) charged V_{Ga} center has a more complicated variation due to the importance of the Fermi-level position. As frequently observed in high bandgap materials, UV photoexcitation at low temperatures allows to modify the equilibrium spin concentrations and is also efficient in this case [Figs. 3(c) and 3(d)].

The increased V_{Ga} EPR spectrum remains stable after the excitation is shut off. In the 1100 °C annealed sample, the V_{Ga} spectrum is no longer observed before photoexcitation but is observed after UV excitation. In the 1200 °C annealed sample, the V_{Ga}^{2-} spectrum is not observed in thermal equilibrium; only a lower intensity spectrum can be generated by UV photoexcitation. This shows that after the 1100 °C anneal the Fermi-level is below its charge transition level (−2/1−) and most of the V_{Ga} centers are in the 1− charge state not observable by EPR. The fraction of the V_{Ga} centers which can be transformed in the EPR active 2− charge state by electron transfer from the VB to

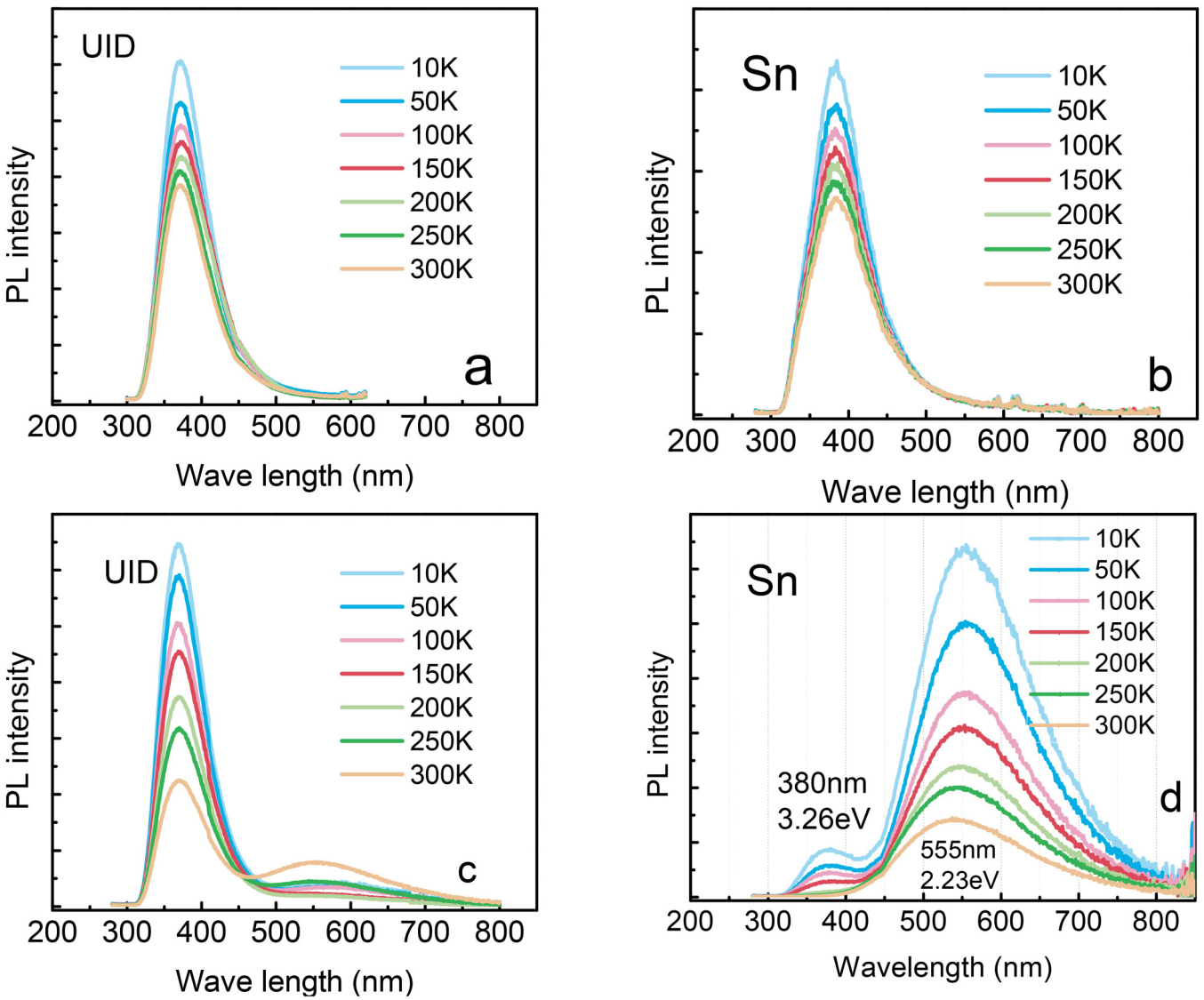

FIG. 4. (a) and (c) PL spectra of the UID sample before (a) and after 1200 °C anneal (c). (b) and (d) PL spectra of the Sn doped sample before (b) and after 1200 °C anneal (d).

the V_{Ga}^{1-} center depends on the light source (wavelength, intensity) and is in competition with photoinduced charge transfer to the impurities Cr, Fe, Cu, and Mn equally present in these samples.[34,35] The spin concentration of the EPR active fraction of V_{Ga} is rather small, of the order of 5×10^{16} cm^{-3}, which is related to the Fermi-level position required for its observation.

We have equally investigated the PL spectra from 10 to 300 K of the UID and Sn doped samples with/without oxygen annealing in the UV and visible spectral range. PL spectra were measured using a 266 nm excitation. This spectrometer uses a xenon lamp as the excitation source. In Ga_2O_3, various PL and CL spectra have been reported.[36–38] They are called the UV, blue, and green bands, which have been tentatively, assigned to O and Ga vacancy centers. In Fig. 4, we show the photoluminescence spectra of the UID and Sn samples before and after 1200 °C annealing. Before annealing, the PL spectra are similar for the two types of samples with the UV band dominating. After the highest annealing of T = 1200 °C, the UID sample shows only the UV band 370 nm and a weak spectrum centered at $\lambda = 550$ nm, whereas the spectrum at 550 nm becomes highly dominating in the Sn doped sample. The broad PL spectrum at 550 nm has not yet been reported and we assign it based on *first-principles* calculations to the recombination on the V_{Ga} defect,

TABLE I. Experimental and theoretical results of EPR parameters (principal values and principal axes of the g-tensor g, hyperfine interaction parameter A) of V_{Ga}^{2-} related centers in β-Ga_2O_3 with two (ib) and three (ic) dominant Ga-ligands. For further details of the Sn related defect structures see also Fig. 5. The difference in the g_{11} values measured here and in Ref. 41 is probably due to an error in the sample orientation in Ref. 41.

Experiment					
V_{Ga} formation	g_{11}	g_{22}	g_{33}	A(^{69}Ga)[G]	Reference
Oxygen annealed at 900 °C < T < 1200 °C	2.0423 0° to **b**	2.0160 −30° to **c**	2.0024 60° to **c**	28.2,28.5 T = 60 K	This work
1450 °C annealed	2.0368 0° to **b**	2.0160 60° to **a**	2.0029 −30° to **a**	28.78,28.78	41
Proton irradiation	2.0312 0°de **b**	2.0079 0°de **c**	2.0026 0° de a*	13.7	39
Proton irradiation + optical excitation	2.0464 0°de **c**	2.0024 0° de **a***	2.0064 0°de **b**	9.8	39
Theory					
Model					
V_{Ga1}–Ga_{ib}–V_{Ga1}	2.0251 0° de **b**	2.0147 70°de a*	2.0048 −20° de a*	−21	33
V_{Ga1}–Ga_{ib}–V_{Ga1}				31.0	41
or V_{Ga1}				32.9	
V_{Ga1}–Sn_{Ga2}	2.0258	2.0073	2.0218	−28.4	
V_{Ga1}–Sn_{ib}–V_{Ga1}	2.0285	2.0153	2.0044	−27.8	
V_{Ga1}–Ga_{ib}–V_{Ga1}–Sn_{Ga2}	2.0265	2.0145	2.0047	−27.3	This work
V_{Ga1}–Sn_{ic}–V_{Ga1}	2.0205	2.0068	2.0205	−26.4 (2×), −25.8 (1×)	
V_{Ga1}–Ga_{ic}–V_{Ga1}–Sn_{Ga2}	2.0230	1.9987	2.0132	−17.2 (2×), −15.9 (1×)	

which as will be shown below, is attributed to a V_{Ga}–Sn complex. In Ref. 38, a PL band with similar wavelength has been theoretically predicted for V_{Ga}–Si complexes.

DEFECT MODELING AND DISCUSSION

Ga vacancy defects, are intrinsic defects, which due to their triple acceptor configuration (3–/2–/1–) will modify the electrical properties of thin films and bulk crystals. In the case of monoclinic *β*-Ga_2O_3 with two distinct Ga lattice sites and three distinct O lattice sites (O_1, O_2, O_3), a variety of Ga vacancy configurations may be formed, as discussed in Refs. 33 and 39–41. In addition to the simple V_{Ga1} und V_{Ga2} configurations, more complex Ga vacancy models such as V_{Ga1}–Ga_i–V_{Ga1} have been proposed.[42] Indeed, scanning transition electron microscopy (STEM) measurements[43] have directly visualized these V_{Ga1}–Ga_i–V_{Ga1} split vacancy complexes. According to *first-principles* calculations, they are more stable than the simple vacancies. V_{Ga} centers. They have been studied by different techniques such as positron annihilation spectroscopy (PA), cathodoluminescence (CL), deep level transient spectroscopy (DLTS), and EPR spectroscopy.[44–47]

Previously, already three different V_{Ga} centers have been evidenced by EPR.[33,39–41] They have been observed after high-energy particle irradiation or high-temperature annealing but were not observed by EPR as native defects. Particle irradiation with energies close to the displacement threshold for Ga or O atoms is a standard technique to generate vacancy defects.[47] V_{Ga} defects are actually oxygen hole centers, where the hole is localized on one of the first nearest oxygen neighbors of the Ga vacancy. A common property of the Ga vacancy defects is a *g*-tensor with principal values $g > 2.00$ and a hyperfine interaction (HF) interaction with two or more nearest neighbor Ga atoms. Proton irradiation, electron irradiation, or neutron irradiation have been shown to generate the same V_{Ga} center, observed by EPR in the paramagnetic 2− charge state. The analysis of its spin Hamiltonian parameters[33] discarded the simple model of a monovacancy and favored the one of a split vacancy complex. Low temperature optical excitation transforms this V_{Ga} center in a different metastable configuration. This photo-excited variant of the V_{Ga} center has also been attributed to a self-trapped hole center,[48] but this model has been discarded recently.[49] The thermal stability of the radiation induced V_{Ga} center is low and they anneal out at temperatures of T > 650 °C.[47]

The V_{Ga} center observed after high-temperature annealing of Sn doped *n*-type material does not fit to any of the previous models discussed in Ref. 33. A similar defect was reported in Si doped and 1450 °C annealed materials,[41] but with slightly different *g*-tensor values. A common key-property of these thermally induced V_{Ga} centers is an increased value of the hf interaction with two Ga neighbors, which is about twice the value of the irradiation induced V_{Ga}^{2-}. The experimental and calculated EPR parameters of the different V_{Ga} centers are compared in Table I.

Our results have shown the importance of the carrier concentration and/or the chemical nature of the dopant, Si or Sn, for the electrical compensation of *n*-type *β*-Ga_2O_3 by high-temperature annealing. As this V_{Ga} center is not observed in the UID doped annealed samples, where the *n*-type conductivity is associated with Si shallow donors, but only in Sn doped samples after annealing we have considered the formation of V_{Ga}–Sn complexes. These defect complexes are EPR-active with spin $S = 1/2$ in the single negative charge states due to the binding with donor atoms. We have calculated the spin properties of the most stable V_{Ga}–Sn complexes in this charge state. Indeed, both Si and Sn donors as well as V_{Ga}

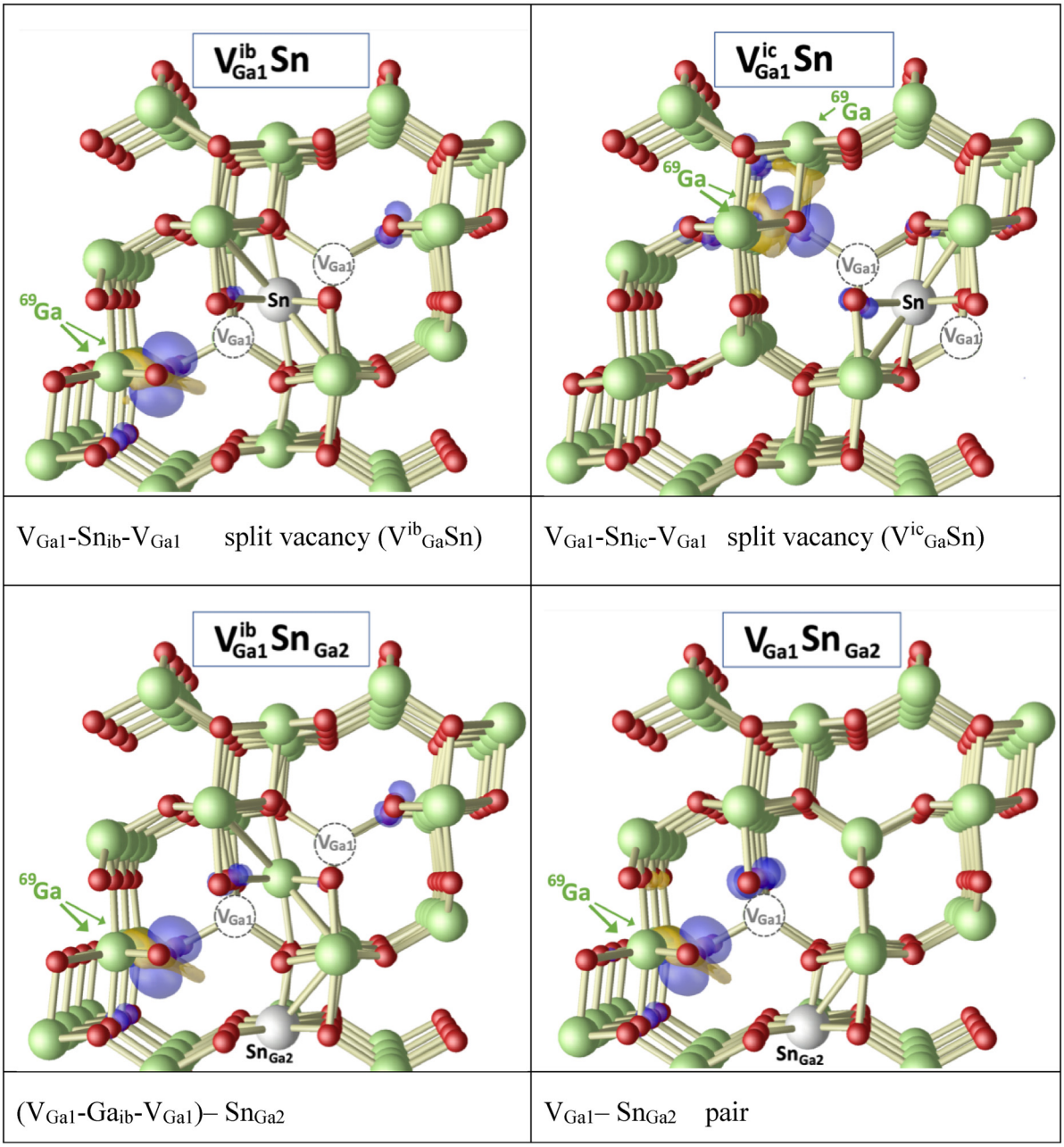

FIG. 5. Models for the most stable $V_{Ga}Sn$ complexes: V_{Ga1}–Sn_{ib}–V_{Ga1} and V_{Ga1}–Sn_{ic}–V_{Ga1} split vacancies (top), nn neighbor V_{Ga1}–Sn_{Ga2} pair (bottom right), and V_{Ga1}–Ga_{ib}–V_{Ga1}–Sn_{Ga2} complex (bottom left). The spin-densities of the unpaired electron predominantly localized at an O1/O3 dangling bond atom are shown in blue (positive values) and yellow (negative values). The latter give rise to the negative hf splittings due to the interaction with two/three dominant ^{69}Ga, ^{71}Ga ligands.

centers have been shown to become mobile at temperatures above T = 1000°C[44,50]; Sn donors diffuse via the formation of Sn–V_{Ga} complexes. We restrict our DFT calculations of V_{Ga}–Sn_{Ga2} complexes to the case of nearest neighbor (nn) configurations. For more distant configurations, there are many different possibilities, with varying distances and orientations, which should give rise to a distribution of EPR parameters. Since in our EPR experiment there is no hint to such a distribution, we limit our calculations to

TABLE II. Comparison of the peak energy of PL bands corresponding to recombination from the CB to the negatively charged defect, resulting in the 2− charge state. The (2−/1−) charge transition level between the paramagnetic 1− and diamagnetic 2− charge state as well as the relative formation energy is also given. The binding energy of V_{Ga1}–Sn_{ib}–V_{Ga1} in the single negative charge state is 1.16 eV; for all other configurations, it is significantly smaller.

Defect	Peak position PL band (eV)	(2−/1−) charge transition level (eV)	Rel. formation energy (eV)
V_{Ga1}–Sn_{Ga2}	1.98	E_{CB}—2.48	+0.81
V_{Ga1}–Ga_{ib}–V_{Ga1}–Sn_{Ga2}	2.11	E_{CB}—2.63	+0.41
V_{Ga1}–Ga_{ic}–V_{Ga1}–Sn_{Ga2}	2.92	E_{CB}—3.28	+0.11
V_{Ga1}–Sn_{ic}–V_{Ga1} ($V^{ic}_{Ga}Sn$)	2.74	E_{CB}—3.35	+0.09
V_{Ga1}–Sn_{ib}–V_{Ga1} ($V^{ib}_{Ga}Sn$)	2.19	E_{CB}—2.64	0.00
Experiment	2.23		

nearest neighbor (nn) complexes. Previous calculations have shown (i) that Sn prefers to occupy the Ga_2 sublattice site, also in the case of pairing with V_{Ga} vacancies, and (ii) $V_{Ga}Sn$ complexes, are more stable in the two split vacancy configurations, V_{Ga1}–Sn_{ib}–V_{Ga1} ($V^{ib}_{Ga}Sn$) and V_{Ga1}–Sn_{ic}–V_{Ga1} ($V^{ic}_{Ga}Sn$), than as a simple nn neighbor pair $V_{Ga1}Sn_{Ga2}$. We have also considered two possibilities not reported before, where the Sn atom does not host the interstitial position of the Sn split vacancy configurations, but changes position with one of the neighboring in-plane Ga_2 lattice sites. From the nn neighbor pair $V_{Ga1}Sn_{Ga2}$ these configurations can be formed gaining energy, if one of the Ga1 neighbors is relaxing toward the V_{Ga1} position, occupying one of the sixfold coordinated ib/ic interstitial sites. According to our HSE total energy calculations, these configurations in their EPR-active 1− charge state are higher in energy than the V_{Ga1}–Sn_{ib}–V_{Ga1} ground state configuration (Fig. 5), but actually by 0.4 eV (V_{Ga1}–Ga_{ib}–V_{Ga1}–Sn_{Ga2}) and 0.8 eV (V_{Ga1}–Ga_{ic}–V_{Ga1}–Sn_{Ga2}) lower in energy than the simple $V_{Ga1}Sn_{Ga2}$ pair.

Our DFT calculations show (Table I) that the models V_{Ga1}–Sn_{ic}–V_{Ga1} and V_{Ga1}–Ga_{ic}–V_{Ga1}–Sn_{Ga2} can be clearly ruled out. In these models, the unpaired electron is localized on a threefold coordinated O_3 atom dangling bond. They would give rise to an additional hf interaction with a third Ga ligand with hf splittings of 25 and 15 G, respectively. This is incompatible with the experimental hf interaction observed in this work. Furthermore, the orientation of the *g*-tensors is different from our results. Although both ic-related complexes provide only slightly enhanced formation energies (∼0.1 eV above the V_{Ga1}–Sn_{ib}–V_{Ga1} ground state), they are obviously not observed in the EPR measurements. According to our total energy calculations, this can be explained by their charge transition levels, which are situated more than 3.2 eV below the conduction band minimum. Assuming a Fermi-level close to midgap, these $Vn_{Ga}Sn$ complexes will be in their diamagnetic 2− charge state, not observable by EPR.

The spin distribution of the other two V_{Ga}-related defect models is only marginally modified by the presence of the Sn donor atom. The unpaired electron is always predominantly localized on an O_1 oxygen atom. The hf splitting calculated for the two equivalent Ga ligands remains almost unaffected and does not allow us to determine the position of the Sn donor atom, also in the case of the nn neighbor V_{Ga1}–Sn_{Ga2} pair. For the latter, however, the calculated *g*-tensor shows an inverted orientation of the g_{22} and g_{33} principal axes. The medium value g_{22} is not oriented along the crystal ***c axis*** (as in experiment), but close to the a^* direction, so that this model can also be excluded. The two remaining models however provide almost the same *g* tensor (see Table I). The largest component of the *g* tensors is nevertheless smaller than the experimental value. This discrepancy might be compared with the case of intrinsic V_{Ga}-related defects, where similarly underestimated g_{11} values have been calculated using almost the same method.[33]

In order to discriminate further between the two remaining models, we have also calculated the related photoluminescence (PL) spectra corresponding to a recombination with an extra electron toward the diamagnetic $(V_{Ga}Sn)^{2-}$ defect. Following Ref. 38, the peak position is computed by assuming recombination of the EPR-active state with a conduction band (CB) electron. In fact, the CB minimum provides for all investigated defects the lowest excited energy level from which PL emission into the diamagnetic 2− ground state configuration is possible. Due to the strong dispersion of the lowest conduction band around the gamma-point, recombination with the EPR-active defect states explains the large width of the PL band. Table II shows the peak positions calculated for the most stable $V_{Ga}Sn_{Ga2}$ complexes. Again, the ic-related split vacancy configurations do not fit to the experimentally observed energy range. It is the model of the V_{Ga1}–Sn_{ib}–V_{Ga1} split vacancy complex that provides the best agreement with the experiment. With a calculated PL peak position of 2.19 eV, it nearly coincides with the experimental value of 2.23 eV. In the EPR-active negative charge state, it provides the lowest formation energy (see also Table II) with a Sn binding energy of 1.16 eV, which further supports the V_{Ga1}–Sn_{ib}–V_{Ga1} model.

CONCLUSION

The electrical compensation of Sn doped *n*-type β-Ga_2O_3 bulk samples by high-temperature annealing under oxygen is attributed to the combined action of V_{Ga1} formation and Sn diffusion giving rise to the formation of V_{Ga}–Sn complexes. These defects, which we attribute to the split vacancy complex V_{Ga}–Sn_{ib}–V_{Ga}, have a high thermal stability and deep charge transition level slightly above midgap, making them interesting for microelectronic applications, where highly resistive layers are required.[5,6] The formation of V_{Ga}–Sn complexes will lead to electrical compensation in two ways: *(i)* due to the acceptor properties of the V_{Ga}–Sn_i–V_{Ga} defect and (ii) the associated reduction of the Sn shallow donor concentration due to the complex formation. The issue whether the difference in the compensation for the Si and Sn doped samples observed in this study is due to the

chemical nature and site occupation of the dopant (Si, Sn) or to the different Fermi-level position has to be investigated in a future study.

ACKNOWLEDGMENTS

The authors gratefully acknowledge the Paderborn Center for Parallel Computing (PC^2) for the provided computational resources, as well as funding by the Deutsche Forschungsgemeinschaft (DFG) from TRR 142/3-2024, Project No. 231447078, support from the French National Agency (ANR) project "GOPOWER" Grant No. CE-50 N0015-01, and the National Natural Science Foundation of China under Grant Nos. 61925110, U23A20358, 62234007, and 62474170. This work was partially carried out at the Center for Micro and Nanoscale Research and Fabrication of USTC.

AUTHOR DECLARATIONS

Conflict of Interest

The authors have no conflicts to disclose.

Author Contributions

H. J. von Bardeleben: Conceptualization (lead); Data curation (lead); Formal analysis (lead); Funding acquisition (equal); Writing – original draft (lead). **Xuanze Zhou:** Conceptualization (equal); Funding acquisition (equal); Investigation (equal). **Jingbo Zhou:** Conceptualization (equal); Investigation (equal). **Guangwei Xu:** Conceptualization (equal); Investigation (equal). **Shibing Long:** Conceptualization (equal); Investigation (equal); Resources (equal). **U. Gerstmann:** Conceptualization (equal); Formal analysis (equal); Funding acquisition (equal); Writing – original draft (equal).

DATA AVAILABILITY

The data that support the findings of this study are available from the corresponding author upon reasonable request.

REFERENCES

[1]M. Tadjer, J. A. Freitas, Jr., J. C. Culbertson, M. H. Weber, E. R. Glaser, A. L. Mock, N. A. Mahadik, K. Schmieder, E. Jackson, J. C. Gallagher, B. N. Feigelson, and A. Kuramata, "Structural and electronic properties of Si and Sn doped (−201) β-Ga_2O_3 in nitrogen and oxygen atmospheres," J. Phys. D: Appl. Phys. **53**, 504002 (2020).
[2]H. J. von Bardeleben, G. He, Y. Wu, and S. Ding, "High temperature annealing of n-type bulk β-Ga_2O_3 electrical compensation and defect analysis the role of gallium vacancies," J. Appl. Phys. **134**, 165702 (2023).
[3]J. Jesenovec, M. H. Weber, C. Pansegrau, M. D. McCluskey, K. G. Lynn, and J. S. McCloy, "Gallium vacancy formation in oxygen annealed β-Ga_2O_3," J. Appl. Phys. **129**, 245701 (2021).
[4]A. Landgorgen *et al.*, "Influence of heat treatments in H_2 and Ar on the E1 center in β-Ga_2O_3," J. Appl. Phys. **131**, 115702 (2022).
[5]X. Zhou, Y. Ma, G. Xu, Q. Liu, J. Liu, Q. He, X. Zhao, and S. Long, "Enhancement mode β-Ga_2O_3U-shaped gate trench vertical MOSFET realized by oxygen annealing," Appl. Phys. Lett. **121**, 223501 (2022).
[6]Q. He, X. Zhou, Q. Li, W. Hao, Q. Liu, Z. Han, K. Zhou, C. Chen, J. Peng, G. Xu, X. Zhao, X. Wu, S. Long, "Selective high resistive zones formed by oxygen annealing for β-Ga_2O_3 Schottky diode applications," IEEE Electron Device Lett. **43**, 1933 (2022).
[7]F. Wu *et al.*, "Enhancing β-Ga_2O_3 diodes with oxygen annealing," Appl. Phys. Express **17**, 036504 (2024).
[8]M. J. Tadjer, C. Fares, N. A. Mahadik *et al.*, "Damage recovery and dopant diffusion in Si and Sn ion implanted β-Ga_2O_3," ECS J. Solid State Sci. Technol. **8**, Q3133 (2019).
[9]T. Yoo, X. Xia, F. Ren, A. Jacobs, M. J. Tadjer, S. Pearton, and H. Kim, "Atomic-scale characterization of structural damage and recovery in Sn ion implanted β-Ga_2O_3," Appl. Phys. Lett. **121**, 072111 (2022).
[10]K. R. Gann, N. Pieczulewski, C. A. Gorsak *et al.*, "Silicon implantation and annealing in β-Ga_2O_3 role of ambient, temperature and time," J. Appl. Phys. **135**, 015302 (2024).
[11]Z. Zhang, E. Farzana, A. R. Arehart, and S. A. Ringel, "Deep level defects throughout the bandgap of (010) β-Ga_2O_3 detected by optically and thermally stimulated defect spectroscopy," Appl. Phys. Lett. **108**, 052105 (2016).
[12]T. H. Yeom, I. G. Kim, B. H. Lee, S. H. Choh, and Y. M. Yu, "Electron paramagnetic resonance characterization of Cr^{3+} impurities in β-Ga_2O_3 single crystals," J. Appl. Phys. **93**, 3315 (2003).
[13]B. E. Kananen, L. E. Halliburton, E. M. Scherer, K. T. Stevens, G. K. Foundos, K. B. Chang, and N. C. Giles, "Electron paramagnetic resonance study of neutral acceptors in β-Ga_2O_3 crystals," Appl. Phys. Lett. **111**, 072102 (2017).
[14]C. A. Lenyk, N. C. Giles, E. M. Scherer *et al.*, "Ir^{4+} ions in β-Ga_2O_3 crystals an unintentional deep donor," J. Appl. Phys. **125**, 045703 (2019).
[15]C. A. Lenyk, T. D. Gustafson, S. A. Basun, L. E. Halliburton, and N. C. Giles, "Experimental determination of the (0/−) level for Mg acceptors in β-Ga_2O_3 crystals," Appl. Phys. Lett. **116**, 142101 (2020).
[16]T. D. Gustafson, J. Jesenovec, C. A. Lenyk, N. C. Giles, J. S. McCloy, M. D. McCluskey, and L. E. Halliburton, "Zn acceptors in β-Ga_2O_3 crystals," J. Appl. Phys. **129**, 155701 (2021).
[17]S. Bhandari and M. E. Zvanut, "Charge trapping at Fe due to midgap levels in Ga_2O_3," J. Appl. Phys. **129**, 085703 (2021).
[18]S. Bhandari, J. L. Lyons, D. Wickramaratne, and M. E. Zvanut, "Optical transitions of neutral Mg in Mg doped Ga_2O_3," APL Mater. **10**, 021103 (2022).
[19]T. D. Gustafson N. C. Giles *et al.*, "Cu^{2+} and Cu^{3+} acceptors in β-Ga_2O_3 crystals a magnetic resonance and optical absorption study," J. Appl. Phys. **131**, 065702 (2022).
[20]T. D. Gustafson, N. C. Giles, B. C. Holloway *et al.*, "Transition metal ions in β-Ga_2O_3 crystals identification of Ni acceptors," J. Appl. Phys. **132**, 185705 (2022).
[21]P. Giannozzi *et al.*, "QUANTUM ESPRESSO: A modular and open source software project for quantum simulation of materials," J. Phys.: Condens. Matter **21**, 395502 (2009).
[22]P. Giannozzi *et al.*, "Advanced capabilities for materials modeling with quantum espresso," J. Phys.: Condens. Matter **29**, 465901 (2017).
[23]J. Heyd, G. E. Scuseria, and M. Ernzerhof, "Erratum: Hybrid functionals based on screened Coulomb potettial," J. Chem. Phys. **124**, 219906 (2006).
[24]C. J. Pickard and F. Mauri, "All electron magnetic response with pseudopotentials: NMR chemical shifts," Phys. Rev. B **63**, 245101 (2001).
[25]C. J. Pickard and F. Mauri, "First principles theory of the EPR g-tensor in solids: Defects in quartz," Phys. Rev. Lett. **88**, 086403 (2002).
[26]J. P. Perdew, K. Burke, and M. Ernzerhof, "Generalized gradient approximation made simple," Phys. Rev. Lett. **77**, 3865 (1996).
[27]H. J. von Bardeleben, J. L. Cantin, A. Parisini, A. Bosio, and R. Fornari, "Conduction mechanism and shallow donor properties in silicon doped ϵ-Ga_2O_3 thin films an electron paramagnetic resonance study," Phys. Rev. Mater. **3**, 084601 (2019).
[28]H. J. von Bardeleben and J. L. Cantin, "Unusual conduction mechanism of n-type β-Ga_2O_3: A shallow donor electron paramagnetic resonance analysis," J. Appl. Phys. **128**, 125702 (2020).
[29]N. T. Son, K. Goto, K. Nomura *et al.*, "Electronic properties of the residual donor in unintentionally doped β-Ga_2O_3," J. Appl. Phys. **120**, 235703 (2016).
[30]A. T. Neal, S. Mou, S. Rafique *et al.*, "Donors and deep acceptors in β-Ga_2O_3," Appl. Phys. Lett. **113**, 062101 (2018).

[31]Q. Sai, H. Cui, C. Xia, H. Qi, M. Pan, A. M. Ahmed, and M. F. Mohamed, "Conduction mechanism and shallow donor defects in Nb-doped β-Ga_2O_3 single crystals," AIP Adv. **14**, 045244 (2024).
[32]Z. Kabilova, C. Kurdak, and R. L. Peterson, "Observation of impurity band conduction and variable range hopping in heavily doped (010) β-Ga_2O_3," Semicond. Sci. Technol. **34**, 03LT02 (2019).
[33]D. Skachkov, W. R. L. Lambrecht, H. J. von Bardeleben, U. Gerstmann, Q. D. Ho, and P. Deák, "Computational identification of Ga-vacancy related electron paramagnetic resonance centers in β-Ga_2O_3," J. Appl. Phys. **125**, 185701 (2019).
[34]I. G. Kim, T. H. Yeom, S. H. Lee, Y. M. Yu, H. W. Shin, and S. H. Cho, "Electron paramagnetic resonance studies of Mn^{2+} ions in β-Ga_2O_3 single crystal," J. Appl. Phys. **89**, 4470 (2001).
[35]J. E. Stehr, M. Jansson, D. M. Hofmann, J. Kim, S. J. Pearton, W. M. Chen, and I. A. Buyanova, "Magneto-optical properties of Cr^{3+} in β-Ga_2O_3," Appl. Phys. Lett. **119**, 052101 (2021).
[36]K. Shimarura, E. G. Villora, T. Ujiie, and K. Aoki, "Excitation and photoluminescence of pure and Si-doped β-Ga_2O_3 single crystals," Appl. Phys. Lett. **92**, 201914 (2008).
[37]Y. K. Frodason, K. M. Johansen, L. Vines, and J. B. Varley, "Self-trapped hole and impurity related broad luminescence in β-Ga_2O_3," J. Appl. Phys. **127**, 075701 (2020).
[38]Q. D. Ho, T. Frauenheim, and P. Deák, "Origin of photoluminescence in β-Ga_2O_3," Phys. Rev. B **97**, 115163 (2018).
[39]H. J. von Bardeleben, S. Zhou, U. Gerstmann, D. Skachkov, W. R. L. Lambrecht, Q. D. Ho, and P. Deak, "Proton irradiation induced defects in β-Ga_2O_3: A combined EPR and theory study," APL Mater. **7**, 022521 (2019).
[40]B. E. Kananen, L. E. Halliburton, K. T. Stevens, G. K. Foundos, and N. C. Giles, "Gallium vacancies in β-Ga_2O_3 crystals," Appl. Phys. Lett. **110**, 202104 (2017).
[41]N. T. Son, Q. D. Ho, K. Goto, H. Abe, T. Ohshima, B. Monemar, Y. Kumagai, T. Frauenheim, and P. Deák, "Electron paramagnetic resonance and theoretical study of gallium vacancy in β-Ga_2O_3," Appl. Phys. Lett. **117**, 032101 (2020).
[42]J. B. Varley, H. Peelaers, A. Janotti, and C. G. Van de Walle, "Hydrogenated cation vacancies in semiconducting oxides," J. Phys.: Condens. Matter **23**, 334212 (2011).
[43]J. M. Johnson, Z. Chen, J. B. Varley *et al.*, "Unusual formation of point defects complexes in the ultrawide-bandgap semiconductor β-Ga_2O_3," Phys. Rev. X **9**, 041027 (2019).
[44]E. Korhonen, F. Tuomisto, D. Gogova, G. Wagner, M. Baldini, Z. Galazka, R. Schewski, and M. Albrecht, "Electrical compensation by Ga vacancies in Ga_2O_3 thin films," Appl. Phys. Lett. **106**, 242103 (2015).
[45]A. Kyrtsos, M. Matsubara, and E. Bellotti, "Migration mechanism and diffusion barriers of vacancies in Ga_2O_3," Phys. Rev. B **95**, 245202 (2017).
[46]Y. K. Frodason, J. B. Varley, K. Magnus, H. Johansen, L. Vines, and C. G. Van de Walle, "Migration of Ga vacancies and interstitials in β-Ga_2O_3," Phys. Rev. B **107**, 024109 (2023).
[47]T.-H. Dang, M. Konczykowski, H. Jaffrès, V. I. Safarov, and H. J. Drouhin, "Modification of β-gallium oxide electronic properties by irradiation with high-energy electrons," J. Vac. Sci. Technol. A **40**, 033416 (2022).
[48]B. E. Kananen, N. C. Giles, L. E. Halliburton, G. K. Foundos, K. B. Chang, and K. T. Stevens, "Self-trapped holes in β-Ga_2O_3 crystals," J. Appl. Phys. **122**, 215703 (2017).
[49]S. Falletta and A. Pasquarello, "Polaron hopping through piecewise-linear functionals," Phys. Rev. B **107**, 205125 (2023).
[50]Y. K. Frodason, P. P. Krzyzaniak, L. Vines, J. B. Varley, C. Van de Walle, and K. M. H. Johansen, "Diffusion of Sn donors in β-Ga_2O_3," APL Mater. **11**, 041121 (2023).